UNIVERSITY *of York*

This is a repository copy of *Design Optimization and Comparative Study of a Novel Halbach Permanent Magnet Vernier Machine with Alternate Flux Bridge*.

White Rose Research Online URL for this paper:
https://eprints.whiterose.ac.uk/195696/

Version: Published Version

Article:

White Rose
university consortium
Universities of Leeds, Sheffield & York

eprints@whiterose.ac.uk
https://eprints.whiterose.ac.uk/

Article

Design Optimization and Comparative Study of a Novel Halbach Permanent Magnet Vernier Machine with Alternate Flux Bridge

Ziqi Huang [1], Aten Man Ho Chau [2], Shuangxia Niu [1,]*, Xing Zhao [3] and Zhiwei Xue [1]

1   Department of Electrical Engineering, Hong Kong Polytechnic University, Hong Kong, China
2   School of Engineering, The University of Edinburgh, Edinburgh EH9 3FB, UK
3   Department of Electronic Engineering, The University of York, York YO10 5DD, UK
*   Correspondence: eesxniu@polyu.edu.hk

Abstract: The purpose of this paper is to investigate the effect of the alternate flux bridge combining Halbach array in Vernier machines. The key novelty is that integrated with the Halbach array PM, the alternate flux bridge design can not only provide a flux path for low-order harmonics but also effectively improve the torque density of the machine. Together with the other three traditional structures under the same overall size, current density, and PM usage, the proposed structure is optimized by genetic algorithm (GA) to maximize the average torque and minimize the torque ripple. With the winding configuration of full-pitch (FP) and short-pitch (SP), the back-EMF, efficiency, power factor, and other performances of four machines with different topologies are analyzed and compared, respectively. With 2D time stepping finite element analysis (FEA) and experimental verification, the torque density of the proposed design reaches 40.11 KNm/m^3, which is significantly higher than that of its existing counterparts.

Keywords: Halbach array; permanent magnet (PM); flux bridge; genetic algorithm (GA)

1. Introduction

With the development of permanent magnet (PM) material, PM machines have attracted a lot of research interest in recent decades. According to the location of PMs, PM machines can be classified as rotor PM machines and stator PM machines. In stator PM machines, the PM material does not need to suffer from centrifugal forces, and the rotor structure is very simple. However, rotor PM machines usually have a much higher torque density and efficiency than stator PM machines. Therefore, rotor PM machines are currently widely used in various industrial applications such as ship propulsion, wind power generation, and electric vehicles [1–5].

In recent decades, various rotor PM arrangements have been proposed, such as surface type [6], spoke type [7], and interior type [8]. Generally speaking, the surface type is the most commonly used in industrial applications because of its simple structure. However, despite relatively greater manufacturing difficulties, spoke and interior types produce higher air gap flux density and associated torque density when under a flux modulation effect. The Vernier motor was first proposed as a precision angle transducer in 1957 and has been developed for more than 60 years [9], with the use of permanent magnets in this type of machine only appearing 20 years ago [10]. Due to the magnetic gear effect under the flux modulation principle, a low-order and high-speed harmonic can be generated, and a high torque density can be obtained for the Vernier machine [11].

To further enhance the torque density of rotor PM Vernier machines, the PM Vernier machine with Halbach array in [12–14], the spoke type PM Vernier machine by taking advantage of flux focusing effect in [15], and a Vernier PM machine with alternating flux barrier design in [16] are proposed. Further, to improve the magnet usage and to

overcome the "flux barrier effect", a Vernier machine with the dual-stator placement was proposed [17–19]. However, this structure is complex and difficult to manufacture. In this paper, a new Halbach array PM Vernier machine with alternative flux bridges in the rotor is proposed and analyzed. On the one hand, the magnetic field can be improved in the proposed structure due to a magnetic-concentrating effect [20]. On the other hand, these bridges improve the PM circuit by providing a flux path for the low pole-pair working magnetic field. This novel topology contributes to higher torque density and lowers torque ripple in the PM Vernier machine.

The main contents of this paper are as follows: Section 2 introduces the structure of the machine and studies its working principle based on the equivalent magnetic circuit theory (EMC). In addition, the function of the magnetic bridge is also shown. In Section 3, four machines with different structures are optimized, and the key parameters are given. In Section 4, 2D time stepping finite element analysis (FEA) is used to simulate and compare the performance of the proposed PM Vernier machine and another three existing machines. Finally, experimental verification and conclusions are given in Section 5.

2. Machine Structure and Force Operation Principle

2.1. Machine Structure and Winding Configuration

In this paper, four different rotor-PM machines are analyzed, optimized, and compared. The cross-sections of different machines are shown in Figure 1. In Structure I, a spoke type PM design is adopted. In Structure II, the spoke type is integrated with a flux barrier, alternate flux bridges are added below rotor pole pieces, and these bridges are connected by an inner yoke. In Structure III, the Halbach array type is combined with the flux barrier design. The proposed machine Structure IV is presented in Figure 1d, in which PMs are placed in the rotor as integrated Halbach array and flux-bridge types. In addition, the 2-pole-pair full-pitch (FP) distributed winding configuration is used, as shown in Figure 2.
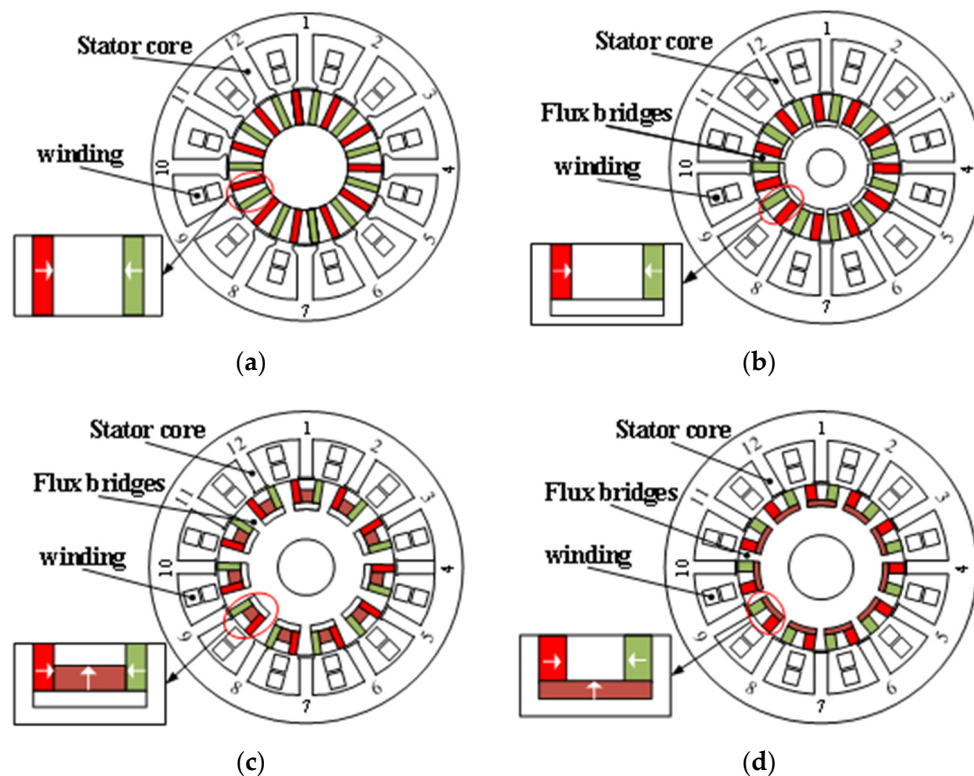

Figure 1. Cross-section of different rotor PM Vernier machines. (**a**) Structure I (Spoke type), (**b**) Structure II (Spoke type with flux barrier), (**c**) Structure III (Halbach array with flux barrier), and (**d**) Structure IV (proposed integrated Halbach array and flux barrier design).
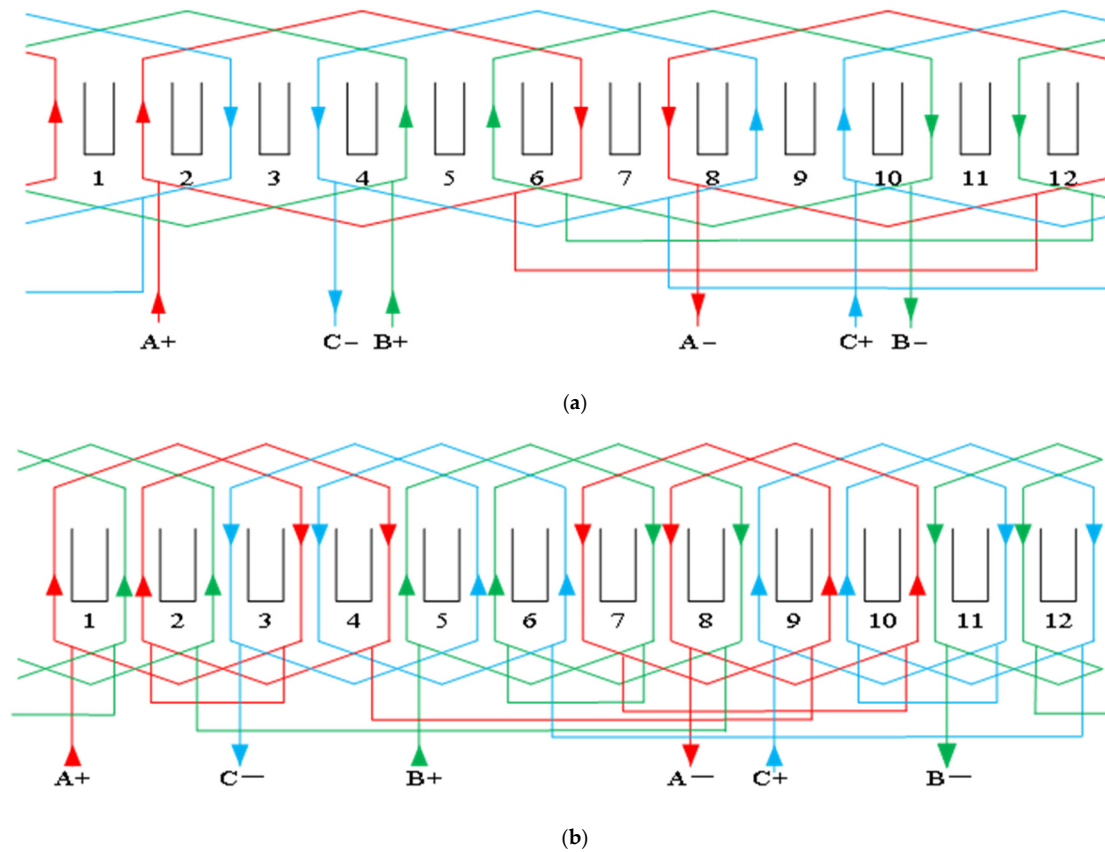
(a)

(b)

Figure 2. Connection of AC armature winding. (**a**) FP winding (**b**) SP winding.

The FP winding configuration (pitch $y_1 = 6$), as shown in Figure 2a, has the disadvantage that the winding end is too long, leading to high copper consumption, low efficiency, and difficult processing. The short-pitch (SP) winding (pitch $y_2 = 3$) configuration shown in Figure 2b will slightly reduce the torque density due to the winding factor decreasing from 0.9659 to 0.683. Moreover, this configuration helps reduce copper consumption and improve the motor's efficiency. The SP winding configuration is selected to be used in the proposed design.

2.2. Operation Principle

To take advantage of the flux-modulation effect of the Vernier machine, the number of winding pole pairs P_w, the rotor pole pairs P_r, and the stator slot Z_s should satisfy

$$P_w = |Z_s - P_r| \tag{1}$$

The MMF produced by the PMs can be expressed as:

$$F_{PMs}(\theta, t) = \sum_{\alpha = 1,2,3\cdots} F_{\alpha m} cos(\alpha P_r(\theta + \phi_r - \Omega_r t)) \tag{2}$$

where $F_{\alpha m}$ is the magnitude of MMF produced by the rotor-PMs; θ is the mechanical angular position; ϕ_r is the initial phase of the rotor.

The rotational angular velocity of the rotor Ω_r can be expressed as:

$$\Omega_r = \frac{2\pi f_E}{P_r} \tag{3}$$

Using Fourier decomposition, the average and fundamental components of the permeance can be expressed as:

$$\Lambda(\theta) = \frac{\Lambda_{0m}}{2} + \sum_{\beta=1,2,3\cdots} \Lambda_{\beta m} cos(\beta Z_s(\theta + \phi_s)) \tag{4}$$

ϕ_s is the initial phase of the stator. From (2) and (4), the air gap flux density can be expressed as:

$$B = F_{PMs}(\theta, t)\Lambda(\theta)$$
$$= \sum_{\alpha=1}^{+\infty} \sum_{\beta=-\infty}^{+\infty} \frac{F_{\alpha m}\Lambda_{|\beta|m}}{2} cos(\alpha P_r(\theta + \phi_r - \Omega_r t) + \beta Z_s(\theta$$
$$+ \phi_s) \tag{5}$$

$$\begin{cases} B_{(\alpha,\beta)} = \dfrac{F_{\alpha m}\Lambda_{|\beta m|}}{2} \\ P_{(\alpha,\beta)} = |\alpha P_r + \beta Z_s|, \alpha = 1, 2, 3\cdots, \beta = 0, \pm 1, \pm 2, \pm 3 \cdots \\ \Omega_{(\alpha,\beta)} = \dfrac{\alpha P_r \Omega_r}{(\alpha P_r + \beta Z_s)} \end{cases}$$

where $B_{(\alpha,\beta)}$ is the amplitude of the modulated flux, $P_{(\alpha,\beta)}$ is the harmonic order, and $\Omega_{(\alpha,\beta)}$ is the rotation speed.

The working harmonic corresponds to the case when $\alpha = 1$. Therefore if the higher-order harmonics are ignored, (5) can be rewritten as:

$$B = F_{PMs}(\theta, t)\Lambda(\theta)$$
$$\approx B_{(1,0)} cos(P_r(\theta + \phi_r - \Omega_r t)) + B_{(1,-1)} cos(P_r(\theta + \phi_r - \Omega_r t) - Z_s(\theta$$
$$+ \phi_s)) + B_{(1,-1)} cos(P_r(\theta + \phi_r - \Omega_r t) + Z_s(\theta + \phi_s)) \tag{6}$$

Due to $\frac{P_r}{Z_s + P_r}$ is very small, so in the case of $(\alpha = 1, \beta = 1)$ often can be ignored.

2.3. Function of Bridge and Magnetic Circuit

It is well known that the back EMF E_0 and average electromagnetic torque T_e of PMV Machines are mainly sourced by 2 air gap magnetic field harmonic, i.e., the P_w-pole-pair field $B_{(1,-1)}$ and P_r-pole-pair field $B_{(1,0)}$. E_0 and T_e can be expressed as:

$$E_0 = \sqrt{2}k_w N_s r_g L_{st} \left(\frac{P_r}{P_w} B_{(1,-1)} + B_{(1,0)}\right) \Omega_r \tag{7}$$

$$T_e = 3\sqrt{2}k_w I_{phase} N_s r_g L_{st} \left(\frac{P_r}{P_w} B_{(1,-1)} + B_{(1,0)}\right) \tag{8}$$

where k_w is the winding factor, N_s is the series coil turns per phase, r_g is the air gap radius, L_{st} is the stack length, and I_{phase} is the RMS value of phase current.

As a PMV machine, P_r is always much larger than P_w [21]. The field $B_{(1,0)}$ is a conventional component existing in tegular PMV machines. But the filed $B_{(1,-1)}$ is depending on amplified by the pole ratio in torque generation. In fact, this additional modulation component is an important factor in enabling the PMV machine to achieve a high torque density. Thus, in the design of the PMV machine, to make better use of the flux modulation effect to obtain better performance, it is necessary to obtain considerable amplitude with a small pole pair number of P_w in modulating the magnetic field.

The magnetic circuit of machine I (spoke type) is shown in Figure 3a. The reluctance of this main magnetic circuit is very large because it needs to pass through 5 PMs and bypass the PMs four times, which would weaken the field and decrease the torque density [22,23]. However, from the flux bridges and rotor core of machines II, III, and IV (proposed) as shown in Figure 3b–d respectively, they provide a magnetic circuit for the

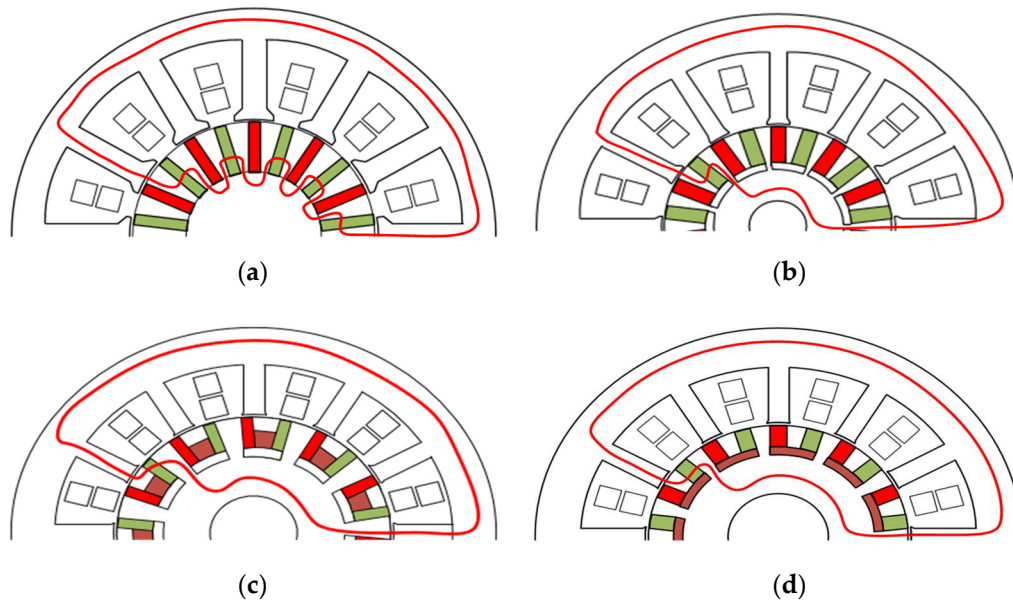low-pole-pair working harmonic and enhance the field which contributes to enhanced torque capability [23].

(a) (b)

(c) (d)

Figure 3. Schematic flux path of PM Vernier machine. (**a**) Structure I, (**b**) Structure II, (**c**) Structure III, and (**d**) Structure IV.

The magnetic circuit of Halbach-array permanent magnets on the rotor is shown in Figure 4. The magnetic fields of the three permanent magnets are concentrated, achieving a better magnetic focus effect. Alongside, there is an air magnetic barrier between the permanent magnet and an inner yoke to prevent a short circuit.
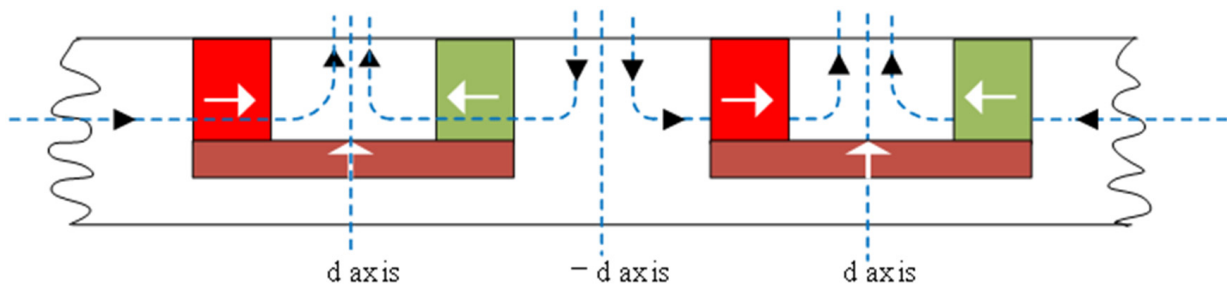

Figure 4. The flux path of the Halbach array PMs on the rotor in the proposed machine.

2.4. Machine Optimization

This section first introduces the optimized logic flow, in which the iterative process based on initial size is shown in detail.

The brief process of optimization is shown in Figure 5. First of all, determining the reasonable range of parameters to be optimized. Secondly, according to the given machine topology and the vibration range of the optimized parameters, the design parameters of the initial generation machine are generated. Then, based on the design parameters, the initial generated finite element model is established, and the finite element calculation and analysis are carried out. Thirdly, a fast non-dominant sort is performed for the initially generated results. If one solution performs better, the solution with poor performance is non-dominant. In this paper, the performance of a solution is evaluated based on whether it has higher torque generation and lower torque ripple. After all the non-dominant solutions are classified, the remaining solutions are added to the Pareto front. For non-initial generation, each solution is compared with the solution in the Pareto front, and the

remaining solutions are updated to the Pareto front after fast non-dominant sorting. Fourth, if the current generation does not reach the maximum generation, a new generation will be generated through selection, crossover, and mutation. Then, repeat the second to fourth steps until the maximum generation is reached and the group with the optimal solution is obtained.
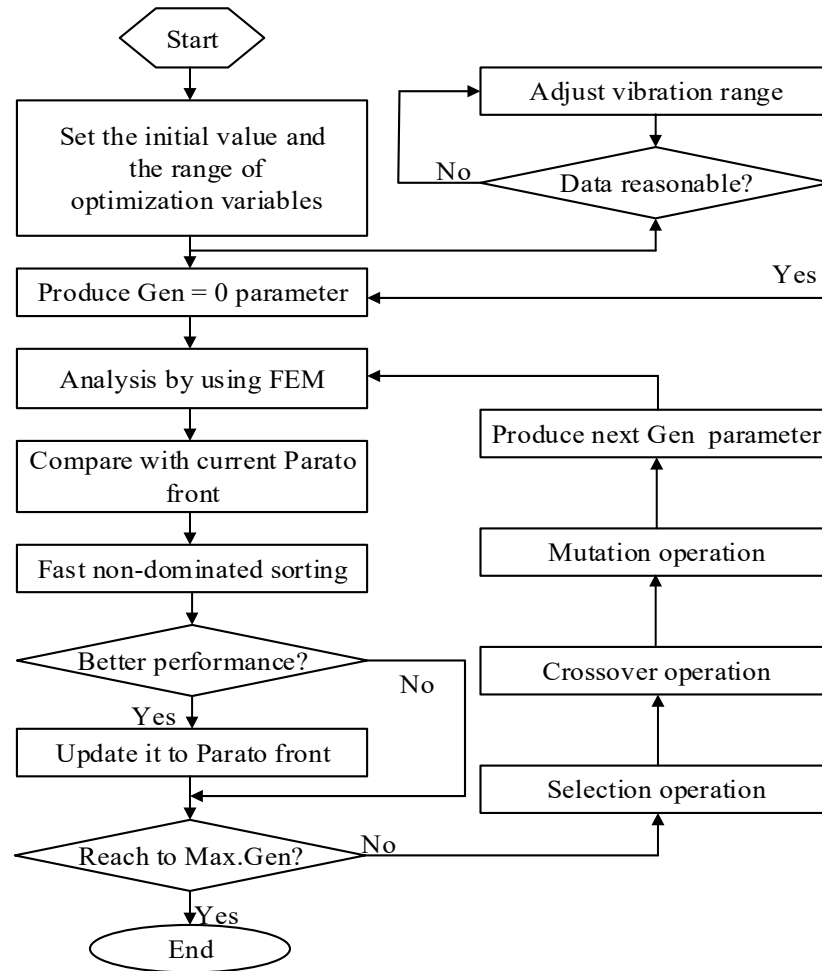
Figure 5. Flow chart of the parameter optimization.

3. Machine Optimization

In this paper, the goal of optimization is to maximize torque and minimize torque ripple. Only one optimal solution is taken for each motor mechanism, and its notations of dimension parameters, dimension parameter of the initial design, design parameter of the optimal machine, and torque performance indexes are shown in Figure 6, Table 1, Table 2, and Table 3, respectively. From Figures 7 and 8, the results show that the maximum torque can be obtained using the proposed motor topology, which preliminarily proves its performance advantages. The next chapter will compare the electromagnetic performance of the four motors in detail.
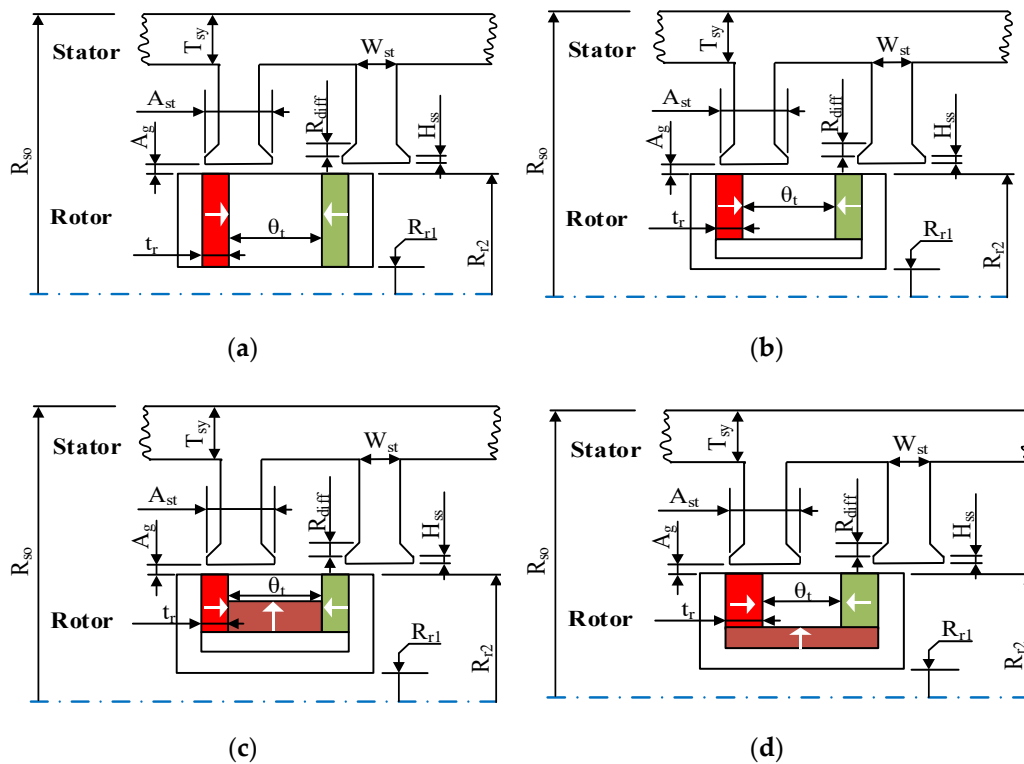
Figure 6. Notations of dimensional parameters. (**a**) Structure I, (**b**) Structure II, (**c**) Structure III, and (**d**) Structure IV.

Table 1. Dimension parameter of the initial design.

Item	Notation	Unit	Value
Stack Length	L_{st}	(mm)	85
Outer radius	R_{so}	(mm)	62
Air gap length	A_g	(mm)	0.8
Rotation speed	S_{pd}	(rpm)	300
Number of turns of armature winding	N_{AC}	/	143
Current density	C_d	A/mm^2	6
Slot filling factor	S_f	/	0.5

Table 2. Optimal dimension parameter with FP wingding configurations.

Item	Notation	Unit	Structure I	Structure II	Structure III	Structure Iv	Vibration Ranges
Stator tooth width	W_{st}	(mm)	7.15	3.89	5.11	5.38	3.5−7.5
Stator yoke height	T_{sy}	(mm)	8.4	10.9	10.5	12.1	7.5−12.5
	R_{diff}	(mm)	1.27	1.4	1.46	0.7	0.4−1.6
Slot open size	A_{st}	(degree)	17.78	9.64	10.53	8.76	5−20
	H_{ss}	(mm)	1.48	0.28	0.63	0.25	0.1−1.8
PMs size	t_r	(mm)	2.92	4.77	3.21	3.99	2.5−5
	θ_t	(degree)	9.4	6.52	5.39	8.76	4−11
Rotor inner radius	R_{r1}	(mm)	17.2	8.61	12.15	13.85	5−20
Rotor outer radius	R_{r2}	(mm)	30.9	32	35.4	33.5	25−35

Table 3. Optimal dimension parameter with SP wingding configurations.

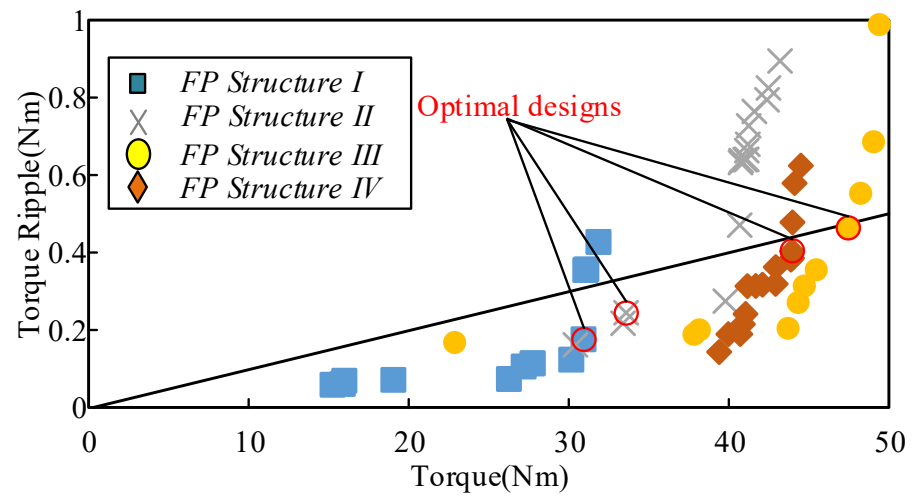| Item	Notation	Unit	Structure I	Structure II	Structure III	Structure IV	Vibration Ranges
Stator tooth width	W_{st}	(mm)	7.74	4.37	3.89	5.05	3.5−7.5
Stator yoke height	T_{sy}	(mm)	8.1	9.9	10.9	10.4	7.5−12.5
Slot open size	R_{diff}	(mm)	1.44	0.83	0.72	1.12	0.4–1.6
	A_{st}	(degree)	14.4	10.2	6.73	8.11	5–20
	H_{ss}	(mm)	1.6	0.97	0.21	0.28	0.1–1.8
PMs size	t_r	(mm)	2.98	3.56	3.14	3.69	2.5–5
	θ_t	(degree)	8.86	8.8	9.74	9.96	4–11
Rotor inner radius	R_{r1}	(mm)	16.08	7.5	9.4	12.32	5–20
Rotor outer radius	R_{r2}	(mm)	29.5	32.6	33	36.3	25–35

Figure 7. Optimization results of the last generation (Pareto front) with FP wingding configurations.
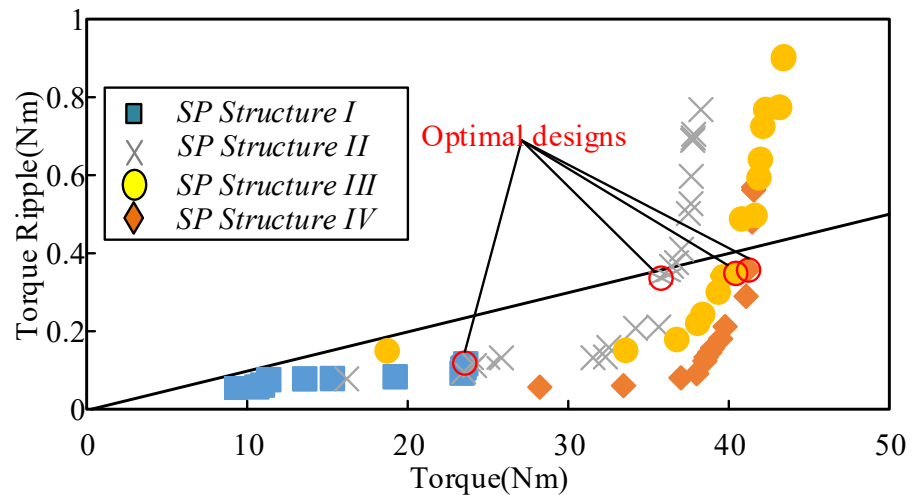

Figure 8. Optimization results of the last generation (Pareto front) with SP winding configurations.

4. Machine Performance Comparison

The structures of four machines are optimized under two different winding configurations, and the optimal size parameters are obtained. This section compares eight cases of both FP and SP winding connections in terms of magnetic field distribution, back electromotive force (EMF), average torque, torque ripple, loss, and efficiency.

4.1. Flux Distribution and Flux Density

Under the SP winding configurations, the flux distribution and flux density of the four machine structures are shown in Figure 9. As shown in Figure 9b–d, the flux bridge provides a flux circuit for low pole-pair permanent magnets. From the perspective of flux density, the stator teeth near the air gap are relatively saturated, and the stator yoke is not saturated. Under the design of FP and SP windings, the flux distribution and density of the four machine structures are almost the same.

Figure 9. Flux distribution and Flux density with SP winding configurations. (**a**) Structure I, (**b**) Structure II, (**c**) Structure III, and (**d**) Structure IV.

With SP winding configurations, the air gap harmonic distributions in four cases are calculated as shown in Figure 10; it includes flux density waveform and correlation harmonic spectrum obtained by fast Fourier analysis. For two different winding configurations, the main working harmonics are the 1st and 11th harmonics, which are highlighted in red and blue, respectively.

4.2. Back EMF

As shown in Figure 11, the amplitudes of even harmonics are very small in every winding method. Since the rotor structure is symmetrical about the d-axis, the air gap MMF is symmetrical, leading to little amplitudes of even harmonics in the air gap MMF. Therefore, the winding flux linkage and associated back EMF have little even harmonics. In terms of the odd harmonics (apart from fundamental harmonic), such as the 3rd and 5th harmonics, their amplitudes are significantly lower than that of the fundamental harmonic because of their low associated winding factor.
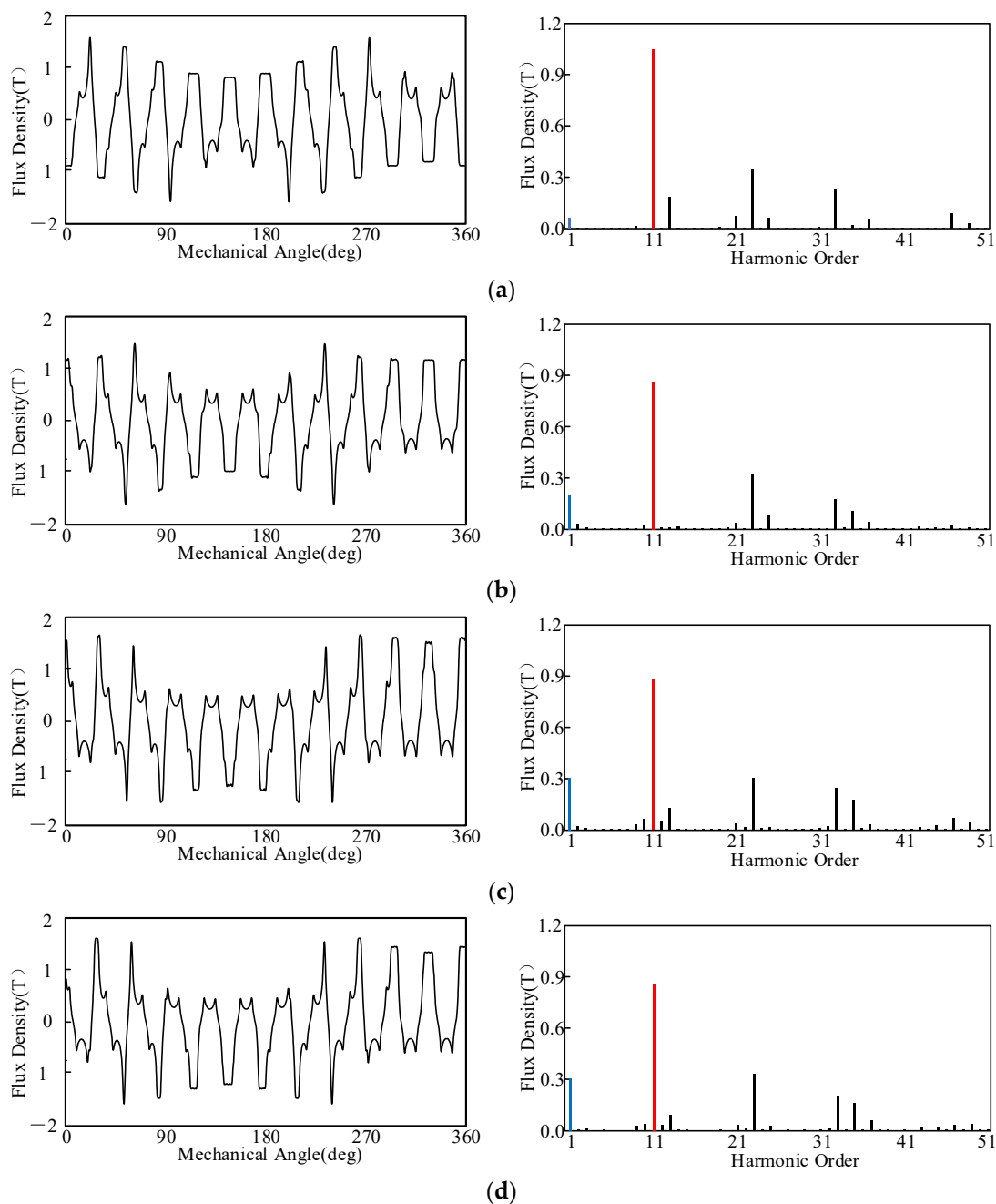
Figure 10. Air gap field and harmonics of PM Vernier machines with SP winding configurations. (**a**) Structure I, (**b**) Structure II, (**c**) Structure III, and (**d**) Structure IV.

4.3. Torque Performance

Considering the same rated current density and the torque ripple of less than 1% as necessary conditions, the torque performance of eight PM Vernier machines is listed in Table 4, including the average torque and torque ripple ratio. As can be seen from the table, when the PM Vernier machines with FP winding configurations, Structure III can obtain the highest average torque. But when the PM Vernier machines with SP winding configurations, the average torque of Structure III and Structure IV are almost the same. No matter what winding configurations, the average torque of Structure I is a relative minimum. In addition, under the same structure, the average torque of the FP winding method is always higher than that of the SP winding connection.
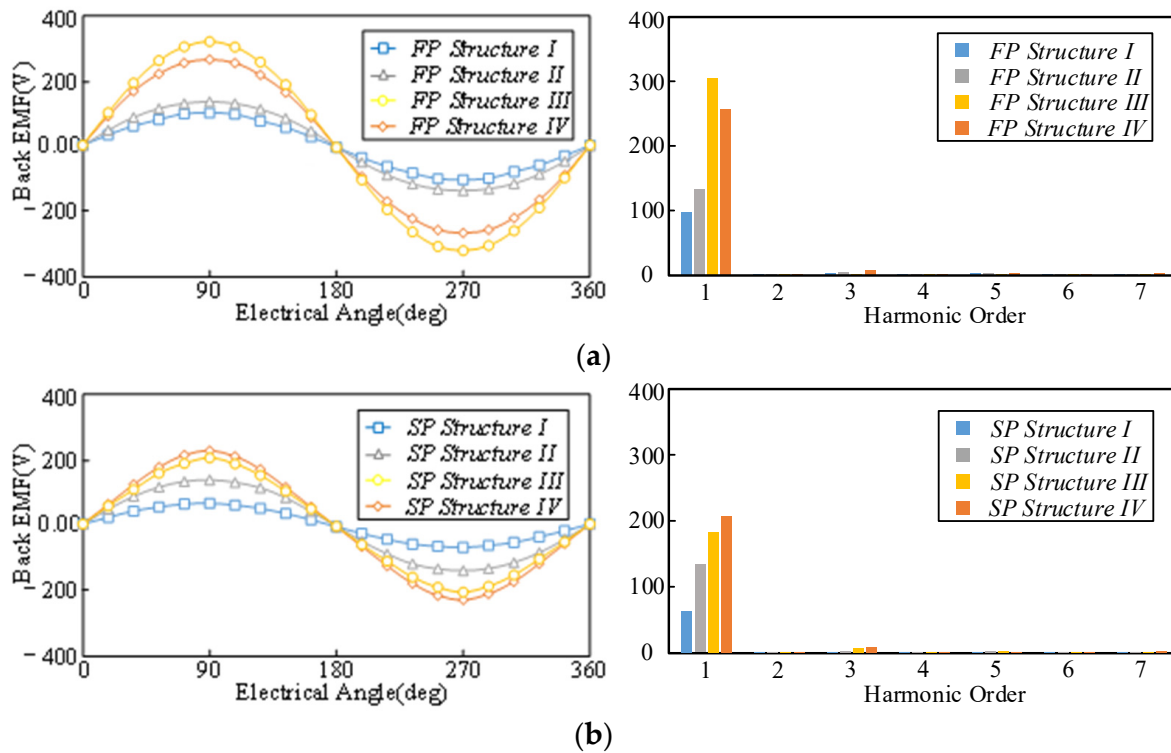
Figure 11. Back EMF with the harmonic distribution. (**a**) PM Vernier machines with FP winding configurations, (**b**) PM Vernier machines with SP winding configurations.

Table 4. Torque Performance.

Winding Configurations	Structure	Average Torque	Value
FP	I	30.92 Nm	0.59%
	II	39.78 Nm	0.61%
	III	47.45 Nm	0.88%
	IV	43.98 Nm	0.98%
SP	I	23.58 Nm	0.49%
	II	36.21 Nm	0.95%
	III	40.42 Nm	0.86%
	IV	41.17 Nm	0.96%

4.4. Loss and Efficiency

Under the same current density, the core loss and efficiency of the eight PM Vernier machines are presented in Figures 12 and 13, respectively, with the speed range from 0 to 2500 rpm. As can be seen from Figure 12, the core loss of Structures II, III, and IV are significantly larger than the traditional Structure I (spoke type) because they have an inner yoke in the rotor. In addition, if it is the same structure, the core loss of the FP winding method is greater than that of the SP winding method. Due to the long magnetic circuit of the armature winding, it is more saturated at the magnetic bridge and stator teeth. At the same time, the copper loss of the FP winding configurations is higher because the end length of the winding increases. Therefore, under the same structure and speed, the efficiency of the SP winding method is slightly higher than that of FP winding.
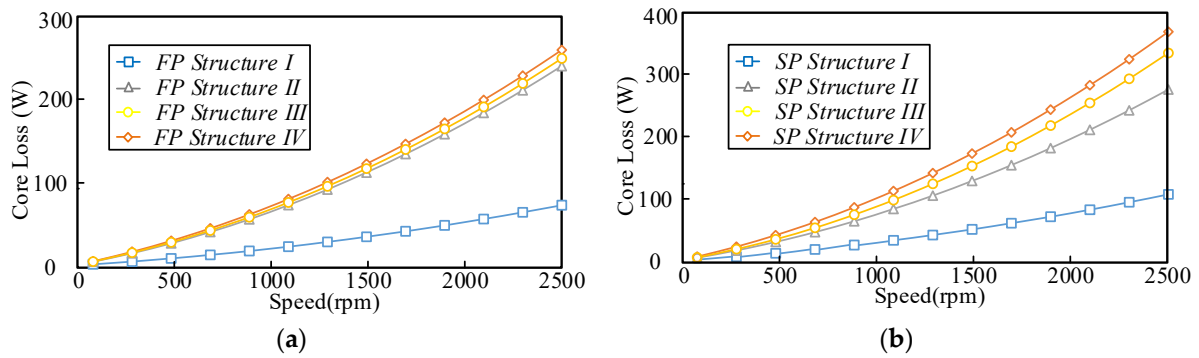
Figure 12. Core loss underrated current density. (**a**) PM Vernier machines with FP winding configurations, (**b**) PM Vernier machines with SP winding configurations.
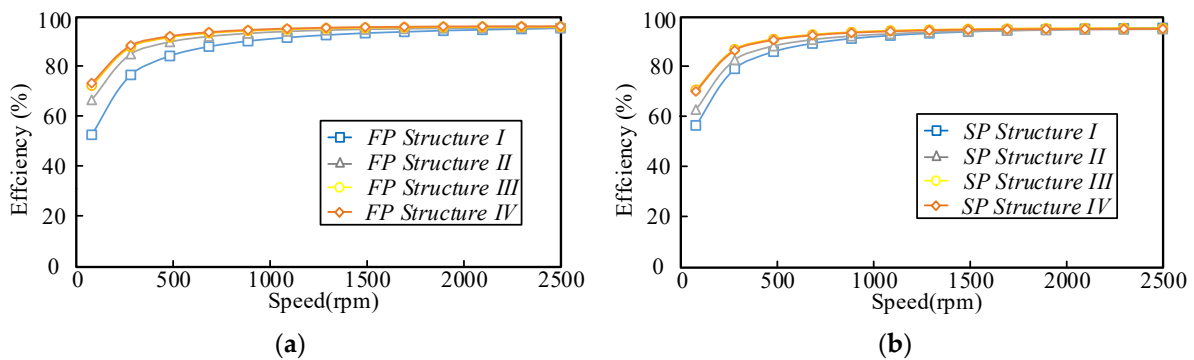

Figure 13. Efficiency underrated current density. (**a**) PM Vernier machines with FP winding configurations, (**b**) PM Vernier machines with SP winding configurations.

4.5. Power Factor

The power factors under different current densities of the eight cases are presented in Figure 14. In general, under the same structure and current density, the power factor in the SP case is higher than that in the FP case. Therefore, it can be admitted that the power factor of the newly proposed Structure III and Structure IV in the case of SP is significantly higher than that of the existing Structure I and Structure II, which reflects the advantages of the new structure.
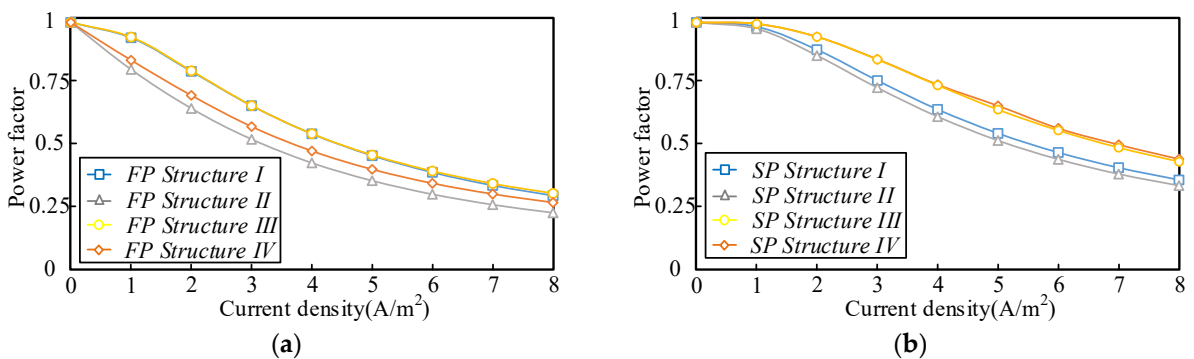

Figure 14. Power factor under different current densities. (**a**) PM Vernier machines with FP winding configurations, (**b**) PM Vernier machines with SP winding configurations.

5. Experiment Validation

To verify the effectiveness of the proposed machine, a prototype is manufactured based on the optimized parameter from the GA. The detail of the prototype and the tested facility is shown in Figure 15. The measured open-circuit back EMF of the prototype is

shown in Figure 16. and the FEA simulation results at 300 rpm. The data show that the experimental results agree with the FEA results. When the armature current is set to the rated value, the torque-current angle curve is measured and shown in Figure 17. It can be seen from the figure that the curve is similar to sine, which is very consistent with the above analysis of winding inductance. When the Id = 0 control method is used, the torque production under different currents is shown in Figure 18. The experimental results show that the torque output is basically the same as in the simulation. The superiority of the proposed model is proven.

Figure 15. The picture of the prototype. (**a**) stator core (**b**) stator with winding (**c**) rotor core (**d**) rotors mechanical connection (**e**) tested bench (**f**) control system.

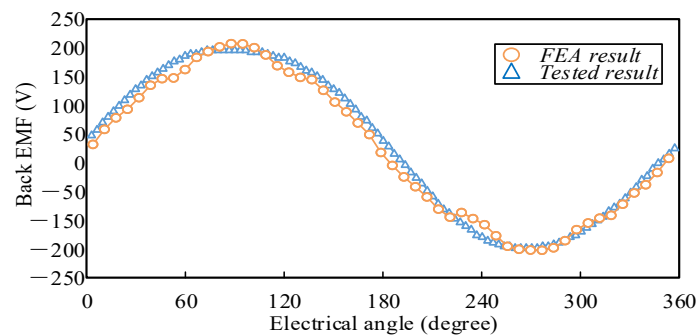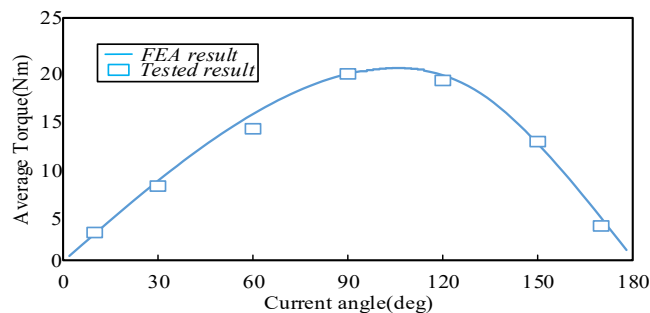**Figure 16.** Tested open-circuit back EMF and FEA results.

Figure 17. Tested output torque and simulated electromagnetic torque.
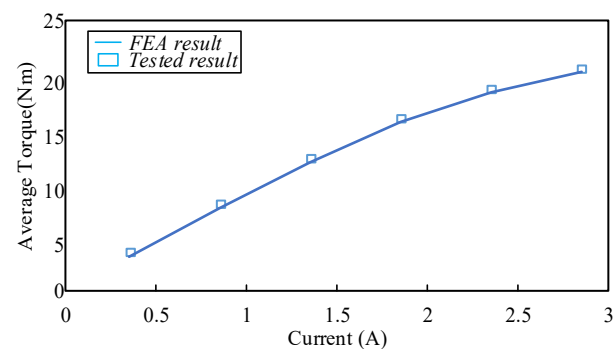

Figure 18. Measured rated output torque and FEA electromagnetic torque under different currents.

6. Conclusions

It was comparatively studied in this paper for a traditional spoke type machine and novel PM Vernier machines with an alternate flux bridge. The topology of the Halbach array integrated with the flux bridge is first presented in this paper. The PM Vernier machines with four different topologies are systematically investigated in two different winding configurations. GA is used to optimize all machines, and their electromagnetic performances are comprehensively researched and compared. The simulation results show that: in general, under the same structure, the FP winding configuration can obtain higher torque density, but due to less copper loss under the SP winding configuration, the efficiency of that is higher. In addition, in the case of SP winding configuration, the torque density of Structure IV is increased by 74.6% and 13.7%, respectively, compared with the existing Structure I and Structure II. From the perspective of efficiency, in the case of low speed, the efficiency of novel Structure III and Structure IV is also higher than that existing in Structure I and Structure II; when the rotor speed is larger than 1500 rpm, the efficiency of all cases are almost the same. Meanwhile, the proposed Structure IV also has an excellent performance in view of the power factor. Although in the case of FP winding configuration,

the power factor is only higher than that of Structure II, and it has the best performance among the four cases under the more appropriate SP conditions for practical application.

References

1. Li, W.; Ching, T.W.; Chau, K.T.; Lee, C.H.T. A Superconducting Vernier Motor for Electric Ship Propulsion. *IEEE Trans. Appl. Supercond.* **2017**, *28*, 5201706. [CrossRef]
2. Li, J.; Chau, K.T.; Jiang, J.Z.; Liu, C.; Li, W. A New Efficient Permanent-Magnet Vernier Machine for Wind Power Generation. *IEEE Trans. Magn.* **2010**, *46*, 1475–1478. [CrossRef]
3. Li, J.; Wu, D.; Zhang, X.; Gao, S. A new permanent-magnet vernier in-wheel motor for electric vehicles. In Proceedings of the 2010 IEEE Vehicle Power and Propulsion Conference, Lille, France, 1–3 September 2010; pp. 1–6. [CrossRef]
4. Hashemnia, N.; Asaei, B. Comparative study of using different electric motors in the electric vehicles. In Proceedings of the 18th International Conference on Electrical Machines, Vilamoura, Portugal, 6–9 September 2008; pp. 1–5. [CrossRef]
5. Choietal, J. Design of high power permanent magnet motor with segment rectangular copper wire and closed slot opening on electric vehicles. *IEEE Trans. Magn.* **2010**, *46*, 2070–2073.
6. Kakihata, H.; Kataoka, Y.; Takayama, M.; Matsushima, Y.; Anazawa, Y. Design of surface permanent magnet-type Vernier motor. In Proceedings of the 2012 15th International Conference on Electrical Machines and Systems (ICEMS), Sapporo, Japan, 21–24 October 2012; pp. 1–6.
7. Han, J.; Zhang, Z. Design and Optimization of a Low-Cost Hybrid-Pole Rotor for Spoke-Type Permanent Magnet Machine. *IEEE Trans. Magn.* **2022**, *58*, 8103105. [CrossRef]
8. Zhao, W.; Zhao, F.; Lipo, T.A.; Kwon, B.I. Optimal design of a novel v-type interior permanent magnet motor with assisted barriers for the improvement of torque characteristics. *IEEE Trans. Magn.* **2014**, *50*, 8104504. [CrossRef]
9. Kronacher, G. Design, Performance and Application of the Vernier Resolver*. *Bell Syst. Tech. J.* **1957**, *36*, 1487–1500. [CrossRef]
10. Ishizaki, A.; Tanaka, T.; Takasaki, K.; Nishikata, S. Theory and optimum design of PM Vernier motor. In Proceedings of the 1995 Seventh International Conference on Electrical Machines and Drives (Conf. Publ. No. 412), Durham, UK, 11–13 September 1995; pp. 208–212.
11. Liu, Y.; Li, H.Y.; Zhu, Z.Q. A high-power factor Vernier machine with coil pitch of two slot pitches. *IEEE Trans. Magn.* **2018**, *54*, 8105405. [CrossRef]
12. Xie, K.; Li, D.; Qu, R.; Gao, Y. A Novel Permanent Magnet Vernier Machine with Halbach Array Magnets in Stator Slot Opening. *IEEE Trans. Magn.* **2017**, *53*, 7207005. [CrossRef]
13. Kataoka, Y.; Takayama, M.; Matsushima, Y.; Anazawa, Y. Design of surface permanent magnet-type vernier motor using Halbach array magnet. In Proceedings of the 18th International Conference on Electrical Machines and Systems (ICEMS), Pattaya, Thailand, 25–28 October 2015; pp. 177–183. [CrossRef]
14. Allahyari, A.; Mahmoudi, A.; Kahourzade, S. High Power Factor Dual-Rotor Halbach Array Permanent-Magnet Vernier Machine. In Proceedings of the 2020 IEEE International Conference on Power Electronics, Drives and Energy Systems (PEDES), Jaipur, India, 16–19 December 2020; pp. 1–6. [CrossRef]
15. Bilal, M.; Ikram, J.; Fida, A.; Bukhari, S.S.H.; Haider, N.; Ro, J.S. Performance Improvement of dual stator axial flux spoke type permanent magnet Vernier machine. *IEEE Access* **2021**, *9*, 64179–64188. [CrossRef]
16. Liu, W.; Lipo, T.A. Alternating flux barrier design of vernier ferrite magnet machine having high torque density. In Proceedings of the 2017 IEEE Electric Ship echnologies Symposium (ESTS), Arlington, VA, USA, 14–17 August 2017; pp. 445–450.
17. Wang, Q.; Niu, S. Design optimization and comparative analysis of dual-stator flux modulation machines. In Proceedings of the IECON 2017—43rd Annual Conference of the IEEE Industrial Electronics Society, Beijing, China, 5–8 November 2017; pp. 3719–3724.

18. Wang, F.; Zhou, L.; Wang, J.; Xiao, Y.; Zhou, J.; Shentu, L. A Novel Dual-Stator Permanent Magnet Vernier Machine with Magnets in Rotor and Both Stators. In Proceedings of the 2018 21st International Conference on Electrical Machines and Systems (ICEMS), Jeju, Republic of Korea, 7–10 October 2018. [CrossRef]
19. Baloch, N.; Kwon, B.-I.; Gao, Y. Low-Cost High-Torque-Density Dual-Stator Consequent-Pole Permanent Magnet Vernier Machine. *IEEE Trans. Magn.* **2018**, *54*, 8206105. [CrossRef]
20. Firdaus, R.N.; Suhairi, R.; Farina, S.; Karim, K.A.; Ibrahim, Z. Improvement of power density spoke type Permanent Magnet Generator. In Proceedings of the 2015 IEEE 11th International Conference on Power Electronics and Drive Systems, Sydney, Australia, 9–12 June 2015; pp. 197–201.
21. Zou, T.; Li, D.; Qu, R.; Jiang, D. Performance Comparison of Surface and Spoke-Type Flux-Modulation Machines with Different Pole Ratios. *IEEE Trans. Magn.* **2017**, *53*, 7402605. [CrossRef]
22. Kim, B.; Lipo, T.A. Analysis of a PM Vernier motor with spoke structure. *IEEE Trans. Ind. Appl.* **2016**, *52*, 217–225. [CrossRef]
23. Ren, X.; Li, D.; Qu, R.; Yu, Z.; Gao, Y. Investigation of Spoke Array Permanent Magnet Vernier Machine with Alternate Flux Bridges. *IEEE Trans. Energy Convers.* **2018**, *33*, 2112–2121. [CrossRef]